



# Surface-electrode ion trap design for near-field microwave quantum gates

James E. Tarlton<sup>1,2</sup> · Richard C. Thompson<sup>1</sup> · David M. Lucas<sup>2</sup>

Received: 28 November 2022 / Accepted: 26 April 2023  
© The Author(s) 2023

## Abstract

We present a design study into an ion trap electrode geometry for applying near-field microwave two-qubit gates. This design features an ‘S’-shaped meander electrode to passively null the microwave field. It has ground planes separating the meander electrode from all of the DC and single-qubit microwave electrodes, which should reduce the sensitivity of the microwave field distribution to the boundary conditions of these electrodes. We show that it is possible to design a single-layer trap with this geometry such that the simulated microwave field null overlaps with the RF field null, and that the positions of these nulls can be simulated to a precision of 100 nm with moderate computing resources. We also show that such a trap can be designed such that ion chains can be trapped, transported and split with feasible DC and RF voltages. While this particular design is optimized for  $^{43}\text{Ca}^+$  ions, our approach could be applied to other ions by changing the microwave frequency to match the corresponding qubit transition frequency.

## 1 Introduction

Quantum computing is an area of technology that promises a range of new abilities above those that are possible with existing, classical, computers [3, 11, 21]. High-fidelity single-qubit [16] and two-qubit [2, 12, 29] gates, as well as long memory times [28] and high-fidelity state preparation and measurement [16], have been achieved in ion trap quantum computing systems. However, while algorithms using small numbers of qubits have been implemented [9, 20, 23], there is still a great deal of progress to be made in scaling systems up to the large sizes necessary for most useful applications.

One approach that may help address this issue is the use of near-field microwaves to perform quantum gates. Microwaves can be produced easily with existing technology, but a strong field gradient is required to entangle ions via their

Coulomb interaction, and the long wavelength means that free-space radiation does not have a sufficiently large field gradient for this. However, the necessary large field gradients can be produced by applying near-field microwaves using electrodes near the ions [24, 25, 35]. In previous work, a gate fidelity close to that of the best laser gates was achieved [17].

A key goal for high-fidelity near-field microwave two-qubit gates is to maximize the ratio of the microwave magnetic field gradient to the microwave magnetic field at the location of the ion. The field gradient is responsible for coupling the internal and motional states of the ions (the precursor to generating entanglement between ions) and the field drives single-qubit operations. Interactions with each individual qubit interfere with two-qubit gates; ideally, one should be able to apply fields or field gradients alone to perform single- or two-qubit gates.

The first experiment on near-field microwave two-qubit gates [25] achieved this by driving three separate linear electrodes with microwave currents. By careful control of the relative amplitudes and phases of these currents, the fields produced by each electrode were made to roughly cancel at the ions’ locations. However, to implement such control is challenging— drifts of the relative amplitudes or phases of the three sources need to be corrected for on a regular basis.

In our previous work [17], we instead drove a single linear electrode which produced a field of a different polarization

✉ James E. Tarlton  
james.tarlton@physics.ox.ac.uk

Richard C. Thompson  
r.thompson@imperial.ac.uk

David M. Lucas  
david.lucas@physics.ox.ac.uk

<sup>1</sup> Department of Physics, Imperial College London, South Kensington Campus, London SW7 2AZ, UK

<sup>2</sup> Department of Physics, University of Oxford, Clarendon Laboratory, Parks Road, Oxford OX1 3PU, UK

to that of our qubit transition. Due to the symmetry of our trap, the central electrode produced a field that was almost entirely  $\pi$ -polarized, which did not directly couple to the  $\sigma$ -polarized qubit transition. However, the field did cause off-resonant excitation of other transitions which are  $\pi$ -polarized, as well as uncontrolled AC Zeeman shifts of the qubit states, resulting in a significant gate error.

Another approach is to have a single electrode to reduce the strict requirements on microwave source amplitude and phase stability, but with multiple linear elements to cancel the field at the ions' locations [6]. This can be achieved with a meander electrode which turns back on itself twice to make an 'S' shape (see figure 1 for an illustration of this). For any microwave amplitude or phase, the resulting microwave field is roughly zero at the same fixed location in the  $x$ - $y$  plane.

The challenge with this approach is in getting the microwave field cancellation to occur in the right place. While a Paul trap can confine ions in a range of locations by adjustment of the DC electrode voltages, the shape of the RF field is fixed by the electrode geometry, which produces a null in the RF field at a single location in the  $x$ - $y$  plane (see figure 1 for direction definitions). Using the DC field to shift ions away from this null results in excess RF micromotion, where the non-zero RF field causes ions to oscillate at the RF frequency. This oscillation generates micromotion sidebands in the ion's spectrum [4], causing significant errors in operations. For ions to experience neither RF micromotion

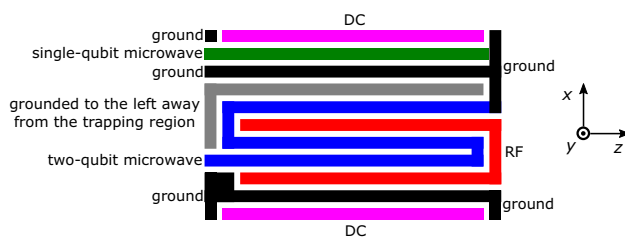


**Fig. 1** Schematic of the trap electrode geometry (not to scale - see Fig. 2 for the actual layout). The blue meander electrode carries the microwave currents for two-qubit gates, the red electrode carries RF voltages, the black electrodes are connected to the ground plane, the green electrode carries the microwave currents for single-qubit gates, and the magenta electrodes carry DC voltages. To simplify the diagram, the two sets of DC electrodes are each combined into single electrodes. The gray electrode is connected to the ground plane further to the left of the figure, 2 mm from the trap center, with a  $5\mu\text{m}$  gap separating it from the ground plane in the trapping region. This separation between the gray electrode and the ground plane suppresses the microwave return currents in this electrode so they instead flow around the electrode, further from the trapping region, which has the effect of moving the microwave field minimum in the negative  $x$  direction, allowing for it to be overlapped with the RF field minimum. The microwave and RF electrodes are connected to their sources to the left and right of the diagrams respectively, with the DC electrodes connected to the top and bottom. The microwave electrodes are connected to the ground plane to maximize the microwave current in these electrodes

nor microwave fields, it is necessary to ensure that the nulls of the RF and microwave fields are in the same place.

Due to their low frequency, RF voltages can be simulated in the same way as DC voltages, meaning that it is easy to accurately predict where the RF field null will be for any given electrode geometry [18, 26, 34]. For microwave currents, the higher frequency means that the current crowds toward the edges of the electrodes (the “skin effect”) in a way that depends upon the exact electrode shapes. While simple electrode structures can be treated analytically, the sort of meander shape necessary for our application must be modeled numerically. We use the simulator HFSS from Ansys, which calculates the fields around electrode structures using the finite-element method. Most of our simulations are performed on a cluster computer run by Advanced Research Computing at the University of Oxford.

For simulations of microwave fields in complex systems, it is not trivial to ensure that the simulation results are accurate while keeping the computational requirements at a manageable level. In addition, the results can be heavily dependent on the boundary conditions of each electrode. Microwave currents from the input electrode couple inductively onto others in the trap structure and reflect back into the trap, as well as producing eddy currents in the other electrodes, generating a secondary microwave field that can cause a significant shift in the location of the field minimum. This depends on the impedance that is attached to those electrodes, which might vary and is dependent on the electrode geometry. Current is also reflected back at the end of the meander, where it terminates at the ground plane. In previous work by another group [31, 32], where the design simulations predicted a separation between the RF and microwave field nulls of  $0.9\mu\text{m}$ , after fabrication and testing, the actual separation was measured to be  $3.8\mu\text{m}$ .

In this paper, we present designs for a meander-electrode trap with a reduced distance between the RF and microwave field nulls to allow for high-fidelity entanglement generation. We present a new geometry which has the meander electrode separated from the electrodes for producing DC trapping fields and microwave fields for single-qubit gates by areas of ground plane. This should reduce the microwave coupling onto these electrodes, which was one of the most significant problems in previous work [31]. In other previous work with a multi-layer design, the introduction of a ground electrode on one side of the meander was shown experimentally to substantially reduce the shift of the magnetic field minimum [15]. Our trap having ground electrodes on both sides should provide even better isolation of the meander electrode.

In addition to the consideration of the field null locations, we also consider the RF and DC voltages necessary for trapping, transporting and splitting ion chains, as well as the trap depth, choosing electrode widths that result in reasonable values for each of these parameters. We investigate the

precision of our simulations by looking at how the simulated field null locations change with increased model resolution, up to the maximum that we can achieve with available computational resources. We also consider how errors in the trap fabrication and changes in trap temperature would change the field distributions.

## 2 Preliminary decisions

Before giving further consideration to the shapes of the trap electrodes, we make some preliminary decisions about the trap. One of the limiting factors in previous work on near-field microwave entanglement generation is the long gate time, as ion heating during the gate results in a significant gate error. This time is limited by the size of the magnetic field gradient at the ions' locations, which can be increased by bringing the ions closer to the trap surface, scaling with the ion height  $d$  as  $\sim 1/d^2$ . However, the ion heating rate would then also increase, scaling as  $\sim 1/d^4$  [5, 10]. We plan for the trap to be cooled with a liquid helium cryostat to  $\sim 20\text{K}$ , which should reduce the ion heating rate by more than an order of magnitude [7, 19]. This would allow the ions to be brought closer to the trap surface. We choose an ion height of  $40\mu\text{m}$ .

We choose gold as the electrode material, which is widely used in surface ion traps. We choose sapphire for the trap substrate material because of its high thermal conductivity at  $20\text{K}$  [14]. This is important for our application as a limitation on two-qubit gate speed is the maximum microwave power that can be dissipated in the trap before thermal transients have a significant effect on experiments. We simulate for a substrate thickness of  $430\mu\text{m}$ , as this is a standard thickness for high-quality sapphire wafers. Sapphire is a uniaxial crystal with one relative permittivity parallel to the  $c$ -axis and another perpendicular to it. We choose the  $c$ -axis to be in the vertical ( $y$ ) direction, as this means that the substrate orientation is unimportant, simplifying the fabrication process.

For the electrode thickness, there are two competing factors. Thicker electrodes spread the microwave currents out more, reducing thermal effects. However, fabrication becomes more challenging with increased electrode thickness. We choose  $8\mu\text{m}$  for the thickness, which should be manageable with existing fabrication techniques [24, 32].

The widths of the electrodes are the main parameters that we vary to achieve our design goals, but we must initially choose a minimum possible width, as fabrication becomes more challenging for smaller electrode widths. We choose a minimum width of  $10\mu\text{m}$ , which has been achieved in several previous surface traps without difficulty [31, 33].

There are several considerations for our choice of the gap width between electrodes. Exposed areas of substrate

can collect charged particles over time, and, due to the high electrical resistivity of the substrate, this charge remains on the surface for long periods, causing drifts in the DC field. This effect is especially problematic for cryogenic environments, as charge mobility is highly suppressed at cryogenic temperatures. To minimize this effect, gaps between electrodes should be as thin as possible. However, if the gaps around the RF electrodes are too thin, electrical breakdown can occur (this is not an issue for the DC electrodes as the DC voltages are much lower than the RF ones), causing damage to the trap. In line with previous work [25, 32, 33], we choose an electrode gap width of  $5\mu\text{m}$ . In areas of the trap further away from the ions, where exposed dielectric has less effect on the trapping field, the electrode gaps could be made wider to improve the fabrication yield.

Depending on the fabrication process, the ratio between the electrode and gap width can be important for the fabrication feasibility and the collection of charges on the exposed substrate. As we have chosen a combination of these two quantities which has been used in previous work (as referenced above), we expect the fabrication to be feasible and the collection of charges to be sufficiently low.

To ensure that our simulations are performed with the correct microwave frequency, we also need to choose the ion species and the qubit transition. We choose  $^{43}\text{Ca}^+$  as the ion, which has previously been used to perform all elementary operations necessary for quantum computing with errors below the threshold required for error correction schemes [8, 16, 17]. We choose the  $|F = 4, M = +1\rangle$  to  $|F = 3, M = +1\rangle$  “atomic clock” transition in the  $4\text{S}_{1/2}$  ground level as our qubit, operating at a magnetic field of  $28.8\text{mT}$ , where the transition frequency is first-order independent of magnetic field. This means that our microwave frequency is  $3.12\text{GHz}$ .

We have already specified that the trap design developed in this design study will feature an ‘S’-shaped meander electrode for carrying microwave currents, but this allows for many different geometries for the RF and ground electrodes. As detailed in Tarlton [30], we considered several possible geometries, performing DC, RF and microwave simulations to investigate the corresponding locations of the RF and microwave field nulls. Based on this investigation, we choose the geometry illustrated in Fig. 1.

Figure 2 shows this geometry with the second microwave electrode and DC electrodes, as implemented in HFSS. The electrodes for producing DC trapping fields and microwave fields for single-qubit gates are separated from the other electrodes by areas of ground plane. In addition, the small size of the gaps between DC electrodes relative to the distance to the trapping zone, as well as the fact that the DC electrode shapes are symmetric about the  $x$ -axis means that the fields from eddy currents along the gaps between the DC electrodes will mostly cancel one another out. Therefore, the details of their shapes have little impact on the location

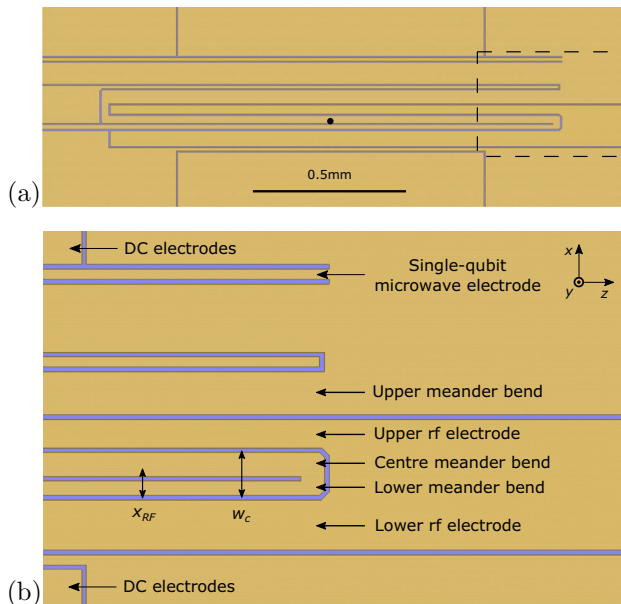


**Fig. 2** **a** The central region of the ion trap design as simulated in HFSS. Each bend of the meander electrode is 1.5 mm long. The electrode immediately above the upper bend of the meander is connected to the ground plane to the left of the area shown, 2 mm away from the trap center. For simplicity, the two sets of DC electrodes are each simulated as single 1 mm-wide electrodes. The central trapping region is indicated with a black circle. **b** A close-up of the right end of the meander (as indicated in the first figure with the dashed line) with each electrode labeled by the names by which they are referred to in this paper. Also denoted are the quantities  $w_c$ , the distance between the two RF electrodes, and  $x_{RF}$ , the horizontal distance between the lower RF electrode and the ions' positions

of the microwave and RF field nulls, and all DC electrodes on either side are combined together into single 1 mm-wide electrodes for simplicity. The single-qubit microwave electrode is set to be adjacent to the upper DC electrode,  $15\mu\text{m}$  wide and  $75\mu\text{m}$  away from the cut in the ground plane near the meander electrode. The microwave current necessary for applying single-qubit gates is much smaller than that needed for applying two-qubit gates, so this electrode can be much further from the ion than the meander electrode. There is a  $15\mu\text{m}$  wide ground electrode between the lower RF and DC electrodes.

There are two main factors to consider in the choice of meander length. We will want to fabricate several trap chips, as there will be some probability of fabrication errors rendering any particular trap unusable, and it would be useful to have one or more extra traps for performing preliminary tests before assembling the final trap apparatus. Therefore, they will be fabricated in batches of small chips on larger sapphire wafers. To fit as many chips as possible on the wafer, the chip, and therefore the meander electrode, should be as small as possible. However, we want to have three trapping regions to allow complex operations to be performed by

transporting ions and performing single- and two-qubit gates on ions in any of the trapping regions. The meander and RF electrodes should be sufficiently short to ensure that end effects are reasonably small in the outer trapping regions. We choose 1.5 mm for the length of each meander bend as a compromise between these competing factors, which would allow for a separation between trapping regions of around  $300\mu\text{m}$ . (The meander length also affects the residual microwave at the field minimum [6], but we find that our chosen length allows for a comparable residual field to previous work (see Sect. 3), so we do not further consider it as a factor in the choice of length.)

### 3 Choice of electrode widths

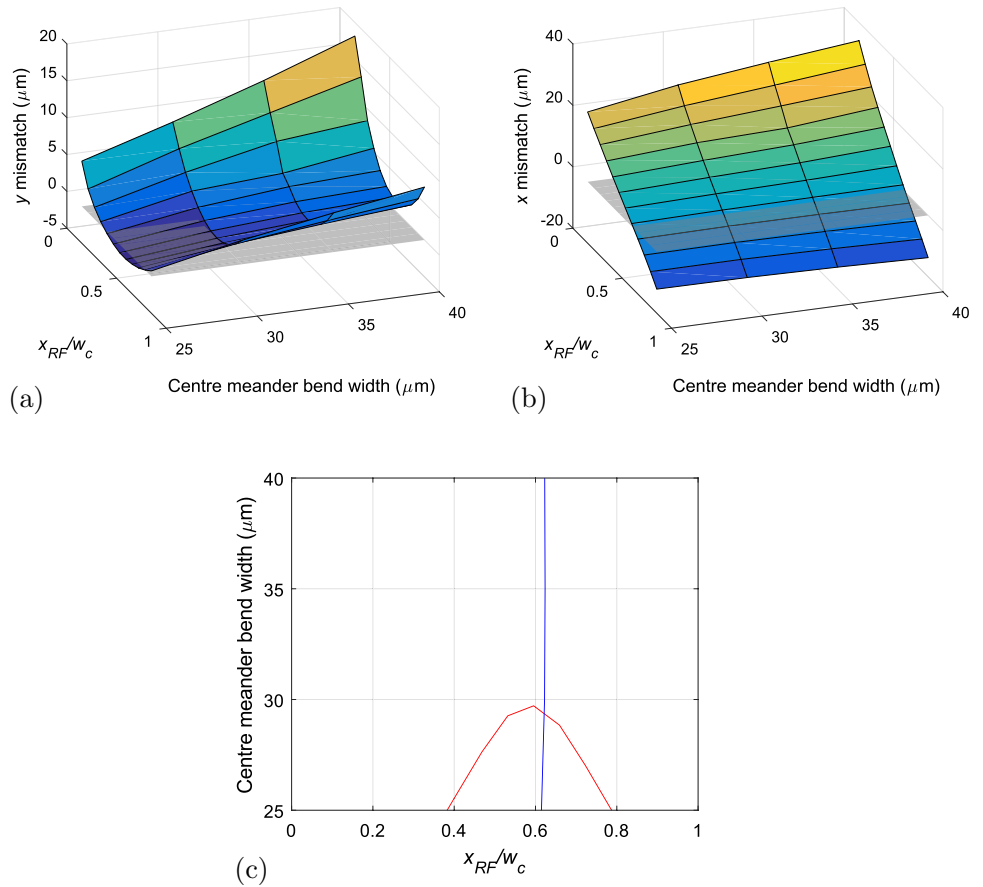
For the chosen electrode geometry, there are five electrodes whose widths have a significant effect on the microwave and/or RF fields: each of the three bends of the meander, and each of the two RF electrodes. There is also the constraint that the RF field null must be  $40\mu\text{m}$  above the electrode surface; we use the House equations [18] to choose RF electrode widths that fulfill this constraint. For each set of electrode widths, we then make a more accurate determination of the RF field null location using HFSS, which deviates from the approximate location by up to a few hundred nanometres.

We scan the different electrode widths to find sets of widths that result in overlapping RF and microwave field nulls. We parametrize the four degrees of freedom with the following four quantities: the width of the center meander bend, how much wider each of the upper and lower meander bends are than the center, and the position of the RF field null in the  $x$  direction. This last parameter, along with the widths of the center and lower meander bends, fully constrains the widths of the two RF electrodes for the chosen ion height of  $40\mu\text{m}$ . We express this parameter as a fraction of the combined widths of the center and lower meander bends (the RF field null must be between the two RF electrodes).

Overlapping the RF and microwave field nulls is the primary objective of the parameter scan, but there are several other factors that will impact the performance of the trap. For the microwave magnetic field, the amplitudes of the field and the field gradient are important, but we find that these quantities do not vary significantly when scanning the different electrode widths.

Other important quantities, which vary significantly with the electrode widths, are the DC and RF voltages required to trap ions, the DC voltages needed to split chains of ions, and the depth of the trapping field. DC and RF simulations, which we present in Tarlton [30], indicate that there is a trade-off between the different parameters. Based on these simulations, we set the distance  $w_c$  between the two RF

**Fig. 3** **a, b** Plots of the mismatch between the microwave and RF field minima in the  $x$  and  $y$  directions as a function of  $x_{RF}/w_c$  and the width of the center bend of the meander electrode, with the lines and surfaces representing linear interpolations between the simulated values. The gray planes show where there is zero mismatch in each direction. **c** The lines in parameter space along which the horizontal (blue) and vertical (red) distances between the two field nulls equal zero. The lower and upper bends of the meander electrode are  $10\mu\text{m}$  thinner and  $20\mu\text{m}$  wider respectively than the center bend (see the main text for an explanation of these choices)



electrodes to be  $50\mu\text{m}$  and the horizontal location of the RF field null  $x_{RF}$  to be around  $30\mu\text{m}$ . These choices allow for ion chains to be trapped, transported and split with feasible DC and RF voltages, as detailed in Tarlton [30], where the widths of the DC electrodes are also presented.

To figure out how to overlap the microwave and RF field nulls while fulfilling these two conditions on the distance between the RF electrodes and the horizontal location of the RF field null, we experimented with varying the different electrode widths, and found that each condition can be met with a single parameter restriction, allowing the other parameters to be varied to overlap the field nulls. We fulfill the former condition by setting the upper bend of the meander electrode to be  $20\mu\text{m}$  wider than the center bend. We fulfill the latter condition by setting the lower bend of the meander electrode to be  $10\mu\text{m}$  thinner than the center bend.

Figure 3 shows the results of the parameter scan for our choices of the widths of the upper and lower bends of the meander electrode. The two remaining parameters are  $x_{RF}$  and the width of the center bend. A linear interpolation of the parameters between the simulation data points gives the electrode widths in Table 1.

The corresponding magnetic field parameters are given in table 2. To put these parameters into context, we note that the ratio between the field gradient and the residual field is

**Table 1** Table of the optimized electrode widths for the design

Electrode	Width ( $\mu\text{m}$ )
Lower bend of meander	19.36
Center bend of meander	29.36
Upper bend of meander	49.36
Lower RF	56.45
Upper RF	34.41

**Table 2** Table of the microwave magnetic field parameters for the electrode widths in Table 1

Parameter	Value
Gradient	$14.9\text{Tm}^{-1}$
Residual field	$10.3\mu\text{T}$

The gradient is calculated using the method detailed in Wahnschaffe [31]. We quote the maximal gradient and assume that the radial secular gate mode can be aligned with this using the DC electrodes. The input power is 1W

$\sim 7$  and  $\sim 100$  times larger than the measured value for our previous trap [27] for  $\sigma$  and  $\pi$  polarizations respectively.

However, compared to the multi-layer trap presented in Hahn et al [15], the field gradient to field ratio is  $\sim 30$  times smaller.

## 4 Simulation accuracy

In this section, we consider possible sources of inaccuracy in the results of our simulations. These could be due to computational resources being insufficient to reach the required level of precision, or due to the HFSS model not being a true representation of the actual trap.

HFSS uses the finite-element method, which means that it divides the model space up into a finite number of elements, or pixels. For each of these pixels, which are tetrahedral in shape, it evaluates the electromagnetic fields. It then increases the number of pixels by splitting some of them into two smaller pixels, and then re-evaluates the fields. This process continues until the specified quantities of interest change by a sufficiently small amount between iterations (called “adaptive passes”), indicating that they have been evaluated to the required level of precision.

Figure 4 shows how the field null coordinates change with each adaptive pass, where the above iterative process continues until the simulation fails to run with our 64GB of RAM. The achieved precision seems to be of order 100nm.

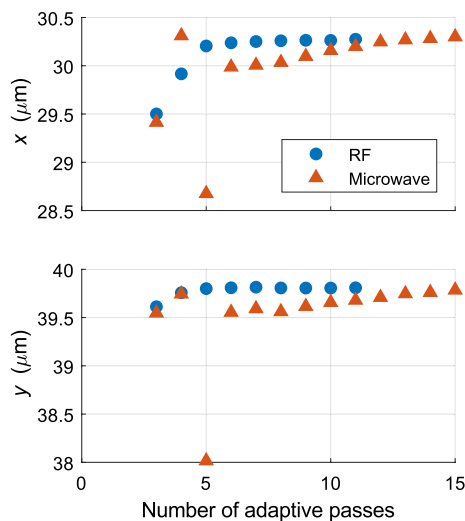


**Fig. 4** Plots showing how the microwave and RF field null coordinates change with the number of adaptive passes completed. The first two adaptive passes give field distributions of poor resolution and are excluded for clarity. The microwave results for the fifth adaptive pass deviate significantly from the others, demonstrating that for low numbers of adaptive passes, the convergence to the correct result is not always smooth. These simulations were carried out with 64GB of RAM, with the computer unable to increase the precision any further than for the final points shown here. Both sets of simulations continue until they run out of RAM, with the RF ones reaching this point after fewer adaptive passes

One of the main reasons for the separation of the RF and microwave field nulls in the meander trap in Wahnschaffe [31] was a large coupling between the meander and single-qubit microwave electrodes, where the coupled microwaves reflected back into the trap in an unpredictable way. We simulated the effects of this coupling in our trap by terminating the single-qubit microwave electrode with either an open or a closed circuit, giving the two extreme situations of how microwaves might be reflected back. The resulting separation between the field nulls is 30nm and 150nm respectively, smaller than the  $3.8\mu\text{m}$  presented in Wahnschaffe [31] and the 170nm presented in Hahn et al [15].

One aspect of the trap that could deviate significantly from the design to the fabricated trap is the electrode dimensions. Our design has  $8\mu\text{m}$ -thick electrodes and  $5\mu\text{m}$  wide gaps between electrodes, but errors in fabrication could result in different values for these parameters. Figure 5 shows how the distance between the microwave and RF field nulls would increase with changes in the electrode dimensions, assuming that the fabrication error is symmetric in all directions. For a fabrication process with an error of  $\sim 1\mu\text{m}$ , the distance between the field nulls could be as large as  $\sim 1\mu\text{m}$ , which, from the field parameters given in Table 2, would roughly double the residual microwave field at the location of the RF field null. Therefore, to ensure that this error were not limiting the performance of the trap, it would be important to use a fabrication process with a smaller error than this.

One other parameter of the trap that we may want to vary is the temperature. The electrical conductivity, and therefore

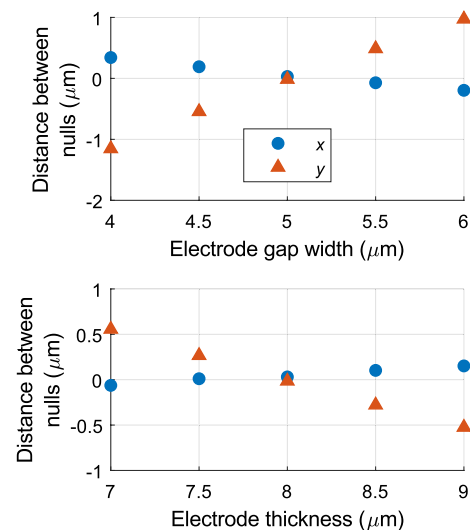


**Fig. 5** Plots showing how the distance between the microwave and RF field nulls changes, in both  $x$  and  $y$ , with the width of the gaps between the electrodes (top) and the thickness of the electrodes (bottom). The distances are defined as the coordinates of the microwave field null minus those of the RF field null

the skin depth, of the electrodes changes with temperature, causing the location of the microwave field minimum to move. Figure 6 shows what the mismatch between the locations of the microwave and RF field nulls would be for 20K, 100K and 300K, which are roughly the temperatures for cooling with liquid helium, cooling with liquid nitrogen or for no cooling respectively. The distance between the nulls increases to only around  $1\mu\text{m}$ , so it would be possible to operate the trap at these temperatures without changing the electrode widths. If the trap were to heat up by a small amount, which might happen from the microwave power going through the meander electrode or from heat deposition in other parts of the system, then the distance between the field nulls would change by a correspondingly small fraction of the amounts shown in the graph.

Finally, as discussed before, the electrical properties of what are connected to the input of all electrodes other than the meander (i.e., the boundary conditions of the HFSS simulations) are important for accurate modeling of the fields. We have chosen a geometry that should have little coupling of microwave currents in the meander electrode to the DC and single-qubit microwave electrodes. For a complete trap design, the boundary condition of the RF electrode would need to be carefully modeled, using methods presented in, for example, Wahnschaffe [31].

## 5 Conclusions

We have presented a design study into a new surface ion trap electrode geometry for achieving high-fidelity near-field microwave two-qubit gates. This geometry features an ‘S’-shaped meander electrode [6] to allow for passive nulling of the microwave magnetic field while still providing a large field gradient. We have designed a trap where the simulated microwave field null overlaps with the RF field null, and simulated the positions of these nulls to a precision

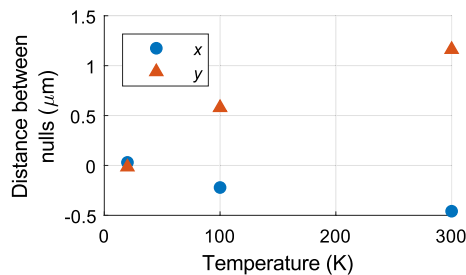


**Fig. 6** Plots showing how the distance between the microwave and RF field null changes, both in  $x$  and in  $y$ , with the temperature of the trap. The only change made to the design between these simulations is an adjustment of the conductivity of the electrodes corresponding to the change in temperature. The distances are defined as the coordinates of the microwave null minus those of the RF null

of  $100\text{nm}$  with  $64\text{GB}$  of RAM. Our design should also allow for ion chains to be trapped, transported and split with feasible DC and RF voltages. It is also worth noting that although this particular design is optimized for  $^{43}\text{Ca}^+$  ions, by changing the microwave frequency to match the corresponding qubit transition frequency, our approach could be applied to other ions.

In previous work on this sort of electrode geometry, the measured distance between the RF and microwave field null was  $3.8\mu\text{m}$  [32]. With such a large distance between these nulls, trapped ions would undergo significant single-qubit rotations during each two-qubit gate and/or experience RF micromotion, both of which would reduce the gate fidelity. The deviation from the simulated value of  $0.9\mu\text{m}$  was attributed to the microwaves applied to the meander electrode coupling to other electrodes and then reflecting back into the trapping region, changing the microwave field distribution in an unpredictable way.

In later work, a ground electrode was introduced on one side of the meander electrode to isolate the meander electrode from one of the two sets of DC electrodes and one of two single-qubit microwave electrodes [15]. The measured distance between the RF and microwave field nulls was  $0.2\mu\text{m}$ , a significant improvement on previous work. Our design has ground electrodes between the meander electrode and all DC and single-qubit microwave electrodes, which should further reduce the sensitivity of the field distribution to the boundary conditions of the electrodes. Our simulations indicate that the separation of the two field nulls resulting from this effect should be less than  $0.2\mu\text{m}$ .

The limiting factor in the performance of our trap design may be fabrication imperfections. A change in the electrode widths or thicknesses of  $1\mu\text{m}$ , which is currently the limit on fabrication tolerances for simple single-layer electroplated traps [31, 33], would substantially change the microwave field distribution, moving the microwave field null away from the RF field null. Because of this sensitivity, we decided instead to use a ‘U’-shaped microwave electrode for future experiments, i.e., a meander with two bends rather than three [33]. Such a trap will not null the microwave field, but it should provide good cancellation of the  $\pi$ -polarized radiation, protecting our  $\pi$ -polarized qubit transition from single-qubit rotations during two-qubit gates. This trap will only be useful for  $\pi$ -polarized qubits, but the field cancellation is expected to be less sensitive to fabrication errors, as well as the boundary conditions of the different electrodes. Using more precise fabrication methods, it should be possible to fabricate our trap design with confidence that fabrication imperfections will not limit the trap performance.

We note that, while we restricted our design study to a single layer of electrodes on the surface trap as this is easier to fabricate, there has been some promising research undertaken in recent years on fabricating surface traps with

multiple layers of electrodes [1, 13, 15, 22]. This has been used to bury microwave waveguides underneath the top layer which then emerge to form electrodes on the surface [15]. Given that microwave systems may be easier to scale to large numbers of qubits than laser systems, and that high-fidelity single- and two-qubit gates have been demonstrated with near-field microwaves [16, 17, 29, 36], the development of new, possibly multi-layer, surface traps featuring microwave electrodes seems to be a promising area of future research.

**Acknowledgements** We are grateful to T.P. Harty for useful discussions. This work was supported by the U.S Army Research Office (ref. W911NF-18-1-0340) and the U.K. EPSRC Quantum Computing and Simulation Hub.

**Author Contributions** JET designed and simulated the ion trap geometry investigated in this research, and drafted the manuscript. DML and RCT supervised the research and contributed to the manuscript.

## Declarations

**Conflict of interest** The authors declare no competing interests.

**Open Access** This article is licensed under a Creative Commons Attribution 4.0 International License, which permits use, sharing, adaptation, distribution and reproduction in any medium or format, as long as you give appropriate credit to the original author(s) and the source, provide a link to the Creative Commons licence, and indicate if changes were made. The images or other third party material in this article are included in the article's Creative Commons licence, unless indicated otherwise in a credit line to the material. If material is not included in the article's Creative Commons licence and your intended use is not permitted by statutory regulation or exceeds the permitted use, you will need to obtain permission directly from the copyright holder. To view a copy of this licence, visit <http://creativecommons.org/licenses/by/4.0/>.

## References

- J.M. Amini, H. Uys, J.H. Wesenberg et al., Toward scalable ion traps for quantum information processing. *New J. Phys.* (2010). <https://doi.org/10.1088/1367-2630/12/3/033031>
- C.J. Ballance, T.P. Harty, N.M. Linke et al., High-fidelity quantum logic gates using trapped-ion hyperfine qubits. *Phys. Rev. Lett.* **117**, 030802 (2016). <https://doi.org/10.1103/PhysRevLett.117.060504>
- P. Benioff, The computer as a physical system: A microscopic quantum mechanical hamiltonian model of computers as represented by turing machines. *J. Stat. Phys.* **22**, 563–591 (1980). <https://doi.org/10.1007/BF01011339>
- D.J. Berkeland, J.D. Miller, J.C. Bergquist et al., Minimization of ion micromotion in a paul trap. *J. Appl. Phys.* **83**, 5025–5033 (1998). <https://doi.org/10.1063/1.367318>
- I.A. Boldin, A. Kraft, C. Wunderlich, Measuring anomalous heating in a planar ion trap with variable ion-surface separation. *Phys. Rev. Lett.* **120**, 02301 (2018). <https://doi.org/10.1103/PhysRevLett.120.023201>
- M. Carsjens, M. Kohonen, T. Dubielzig et al., Surface-electrode paul trap with optimized near-field microwave control. *Appl. Phys. B* **114**, 243–250 (2014). <https://doi.org/10.1007/s00340-013-5689-6>
- J. Chiaverini, J.M. Sage, Insensitivity of the rate of ion motional heating to trap-electrode material over a large temperature range. *Phys. Rev. A* (2014). <https://doi.org/10.1103/PhysRevA.89.012318>
- D.P.L.A. Craik, N.M. Linke, M.A. Sepiol et al., High-fidelity spatial and polarization addressing of 43ca+ qubits using near-field microwave control. *Phys. Rev. A* **95**, 022337 (2017). <https://doi.org/10.1103/PhysRevA.95.022337>
- S. Debnath, N.M. Linke, C. Figgatt et al., Demonstration of a small programmable quantum computer with atomic qubits. *Nature* **536**, 63 (2016). <https://doi.org/10.1038/nature18648>
- L. Deslauriers, S. Olmschenk, D. Stick et al., Scaling and suppression of anomalous heating in ion traps. *Phys. Rev. Lett.* **97**, 103007 (2006). <https://doi.org/10.1103/PhysRevLett.97.103007>
- R.P. Feynman, Simulating physics with computers. *Int. J. Theor. Phys.* **21**, 467–488 (1982). <https://doi.org/10.1007/BF02650179>
- J.P. Gaebler, T.R. Tan, Y. Lin et al., High-fidelity universal gate set for 9be+ ion qubits. *Phys. Rev. Lett.* **117**, 060505 (2016). <https://doi.org/10.1103/PhysRevLett.117.060505>
- N.D. Guise, S.D. Fallek, K.E. Stevens et al., Ball-grid array architecture for microfabricated ion traps. *J. Appl. Phys.* **117**, 174901 (2015). <https://doi.org/10.1063/1.4917385>
- E.A. Gutierrez-D, M.J. Deen, C.L. Claeys, *Low temperature electronics: physics, devices, circuits, and applications* (Academic Press, 2001)
- H. Hahn, G. Zarantonello, A. Bautista-Salvador et al., Multi-layer ion trap with three-dimensional microwave circuitry for scalable quantum logic applications. *Appl. Phys. B: Lasers Opt.* **125**, 1 (2019). <https://doi.org/10.1007/s00340-019-7265-1>
- T.P. Harty, D.T.C. Allcock, C.J. Ballance et al., High-fidelity preparation, gates, memory, and readout of a trapped-ion quantum bit. *Phys. Rev. Lett.* **113**, 220501 (2014). <https://doi.org/10.1103/PhysRevLett.113.220501>
- T.P. Harty, M.A. Sepiol, D.T.C. Allcock et al., High-fidelity trapped-ion quantum logic using near-field microwaves. *Phys. Rev. Lett.* **117**, 030802 (2016). <https://doi.org/10.1103/PhysRevLett.117.140501>
- M.G. House, Analytic model for electrostatic fields in surface-electrode ion traps. *Phys. Rev. A* **78**(033), 402 (2008). <https://doi.org/10.1103/PhysRevA.78.033402>
- J. Labaziewicz, Y. Ge, D.R. Leibbrandt et al., Temperature dependence of electric field noise above gold surfaces. *Phys. Rev. Lett.* (2008). <https://doi.org/10.1103/PhysRevLett.101.180602>
- N.M. Linke, D. Maslov, M. Roetteler et al., Experimental comparison of two quantum computing architectures. *PNAS* **114**, 3305–3310 (2017)
- Y.I. Manin, Vychislimoe i nevychislimoe (Computable and Non-computable). *Sovetskoe Radio* (1980)
- P. Maunz, High optical access trap 2.0. <https://doi.org/10.2172/1237003>, URL <http://prod.sandia.gov/techlib/access-control.cgi/2016/160796r.pdf> (2016)
- T. Monz, D. Nigg, E.A. Martinez et al., Realization of a scalable shor algorithm. *Science* **351**, 1068–1070 (2016). <https://doi.org/10.1126/science.aad9480>
- C. Ospelkaus, C.E. Langer, J.M. Amini et al., Trapped-ion quantum logic gates based on oscillating magnetic fields. *Phys. Rev. Lett.* **101**(090), 502 (2008). <https://doi.org/10.1103/PhysRevLett.101.090502>
- C. Ospelkaus, U. Warring, Y. Colombe et al., Microwave quantum logic gates for trapped ions. *Nature* **476**, 181–184 (2011). <https://doi.org/10.1038/nature10290>
- R. Schmied, J.H. Wesenberg, D. Leibfried, Optimal surface-electrode trap lattices for quantum simulation with trapped ions. *Phys. Rev. Lett.* **102**, 233002 (2009). <https://doi.org/10.1103/PhysRevLett.102.233002>

27. M.A. Sepiol, A high-fidelity microwave driven two-qubit quantum logic gate in  $43\text{Ca}^+$ . URL <https://ora.ox.ac.uk/objects/uuid:9cafc3e-32c2-41dc-874d-632dcc402428> (2016)
28. M.A. Sepiol, A.C. Hughes, J.E. Tarlton et al., Probing qubit memory errors at the part-per-million level. *Phys. Rev. Lett.* **123**, 110503 (2019). <https://doi.org/10.1103/physrevlett.123.110503>
29. R. Srinivas, S.C. Burd, H.M. Knaack et al., High-fidelity laser-free universal control of trapped ion qubits. *Nature* **597**, 209–213 (2021). <https://doi.org/10.1038/s41586-021-03809-4>
30. J.E. Tarlton, Probing qubit memory errors at the  $10^{-5}$  level. URL <https://spiral.imperial.ac.uk/handle/10044/1/60650> (2018)
31. M. Wahnschaffe, Engineered microwave control for trapped ions. URL <https://www.tib.eu/en/search/id/TIBKAT%3A863830021/Engineered-microwave-control-for-trapped-ions/> (2016)
32. M. Wahnschaffe, H. Hahn, G. Zarantonello et al., Single-ion microwave near-field quantum sensor. *Appl. Phys. Lett.* **110**, 034103 (2017). <https://doi.org/10.1063/1.4974736>
33. M.A. Weber, C. Löschnauer, J. Wolf et al, Cryogenic ion trap system for high-fidelity near-field microwave-driven quantum logic. [arXiv:2207.11364](https://arxiv.org/abs/2207.11364) (2022)
34. J.H. Wesenberg, Electrostatics of surface-electrode ion traps. *Phys. Rev. A* **78**, 1–12 (2008). <https://doi.org/10.1103/PhysRevA.78.063410>. [arXiv:0808.1623](https://arxiv.org/abs/0808.1623)
35. D.J. Wineland, C. Monroe, W.M. Itano et al., Experimental issues in coherent quantum-state manipulation of trapped atomic ions. *Journal of Research of the National Institute of Standards and Technology* **103**, 259 (1998). <https://doi.org/10.6028/jres.103.019>, URL <http://nvlpubs.nist.gov/nistpubs/jres/103/3/j33win.pdf>
36. G. Zarantonello, H. Hahn, J. Morgner et al., Robust and resource-efficient microwave near-field entangling  $9\text{Be}^+$  gate. *Phys. Rev. Lett.* (2019). <https://doi.org/10.1103/PhysRevLett.123.260503>

**Publisher's Note** Springer Nature remains neutral with regard to jurisdictional claims in published maps and institutional affiliations.